

Multiview Supervision By Registration

Yilun Zhang
University of Pennsylvania
zhyilun@seas.upenn.edu

Hyun Soo Park
University of Minnesota
hspark@umn.edu

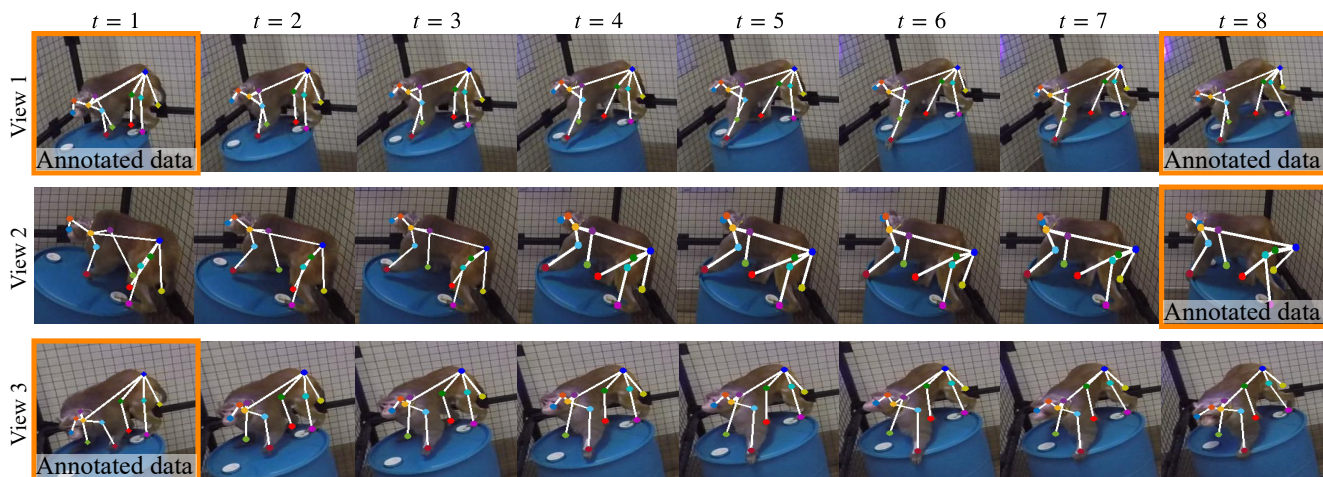


Figure 1: This paper presents a semi-supervised learning framework to train a keypoint pose detector using multiview image streams given the limited number of labeled data. A subset of images at the first and end time instances are labeled where the pose detector trained by multiview cross-supervision results in reliable monkey tracking in 3D.

Abstract

This paper presents a semi-supervised learning framework to train a keypoint pose detector using multiview image streams given the limited number of labeled data (typically $<4\%$). We leverage the complementary relationship between multiview geometry and visual tracking to provide three types of supervisory signals for the unlabeled data: (1) pose detection in one view can be used to supervise that of the other view as they must satisfy the epipolar constraint; (2) pose detection must be temporally coherent in accordance with its optical flow; (3) the occluded keypoint from one view must be consistently invisible from the near views. We formulate the theory of multiview supervision by registration and design a new end-to-end neural network that integrates these supervisory signals in a differentiable fashion to incorporate the large unlabeled data in pose detector training. The key innovation of the network is the ability to reason about the visibility/occlusion, which is indicative of the degenerate case of detection and tracking. Our resulting pose detector shows considerable out-performance comparing the state-of-the-art pose detectors in terms of accuracy (keypoint detection) and precision (3D

reconstruction). We validate our approach with challenging realworld data including the pose detection of non-human species such as monkeys and dogs.

1. Introduction

The ability to automatically parse motor behaviors in relation to the neural signals give rise to an enabling factor of computational neuroscience. In particular, human surrogate models, such as rhesus macaques (monkeys), have been studied to establish the neural-behavioral link through their free-ranging behaviors (including several social behaviors), which is largely homologous to humans. Unfortunately, these experiments have in the past been extremely limited by the requirement that the animal's head be immobile and attached to a large recording rig [28]. 3D pose reconstruction of the behaviors for these models using visual data [13, 19] is completely non-invasive, and therefore, is a viable solution.

Existing pose detectors [7, 20, 26, 30] have been built upon large-scale labeled datasets manually annotated by crowd workers (such as on Amazon Mechanical Turk) [17].

While such detectors have shown highly effective performance on human subjects, applying the detectors to non-human species is challenging because no large labeled dataset exists. More importantly, attaining such annotated data (nearly 2 million instances) is practically infeasible due to three reasons: (a) internet images of non-human species do not represent their visual appearance in the experimental apparatus; (b) a large visual intra-class variations exist, e.g., rhesus macaques vs. mandrill; and (c) annotation tasks require expert primatological knowledge, i.e., non-expert crowd workers and mechanical turkers are not eligible for the annotation tasks. Building a pose detector with small amount of data introduces a strong bias in the trained model because the required number of the training data is known to be equivalent to that of the perceptrons [34]. This fundamentally precludes from enabling 3D pose estimation for these subjects.

This paper proposes a new semi-supervised learning approach for a pose detector that leverages the complementary relationship between multiview geometry and visual tracking to address the limited number of the labeled data. Inspired by the multiview 3D tracking [10, 14, 32] that reliably reconstructs a 3D trajectory with minimal drift, we design an end-to-end neural network that is trained by self-supervisory signals in three ways. (1) Multiview supervision: the pose recognition from two views must satisfy the epipolar constraint. This allows cross-view supervision where recognition in one image can supervise other [13]. (2) Temporal supervision: consecutive images provide an auxiliary supervisory signal [8, 31], i.e., current frame image can be reconstructed by a dense inverse compositional mapping from the next frame. (3) Visibility supervision: precisely reasoning about the occlusion of a keypoint is important because it prevents from learning degenerate cases of tracking and detection, e.g., learning from occluded hands that introduce tracking error. Spatial proximity of cameras can provide a supervisory signal for visibility, i.e., an occluded keypoint from one camera is likely to be invisible from the nearby cameras [14].

Our system takes as an input set of multiview image streams with a small set of labeled data, and outputs a geometrically consistent pose of the subject as shown in Figure . We train a pose detector that minimizes three losses: cross-entropy loss for labeled prediction, geometry reprojection error measured by epipolar divergence [13], and inverse compositional mapping (optical flow) error between consecutive frames. The network is augmented with a novel visibility layer called Visibility Probability Mask that accounts for the validity of the prediction using recognition confidence and spatial proximity of the cameras in 3D. We demonstrate that this semi-supervised learning framework can effectively benefit from the multiview image streams by spatiotemporally intertwining all images together. The

resulting network significantly outperforms state-of-the-art approaches in terms of accuracy (keypoint detection) and precision (3D reconstruction).

Unlike existing multiview supervision approaches [21, 23, 24], our approach inherits the flexible nature of epipolar geometry, which can be applied to various camera pose configurations. We also eliminate the requirement of 3D reconstruction that involves with alternating reconstruction [4, 6, 25, 29] or data driven depth prediction [15, 27, 33] which often suffer from suboptimality. Finally, our design is network-agnostic, i.e., any pose detector producing a probability map representation [7, 20, 26, 30] can be used with a trivial modification.

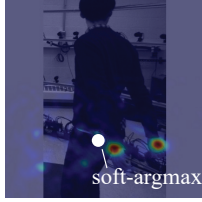
To our best knowledge, this is the first paper that leverages the underlying spatiotemporal constraint of multiview images streams to train a pose detector using large-scale unlabeled data. The core contributions include: (1) a new differentiable formulation of multiview spatiotemporal self-supervision for the unlabeled data; (2) its realization using an end-to-end network that is flexible to camera pose configurations; (3) a visibility layer conditioned on camera spatial proximity and recognition confidence that predicts the occlusion, which enables a precise inference on degenerate keypoints; and (4) strong performance on the realworld data of non-human species on monkeys and dogs with an extremely small set of the labeled data (<4%).

2. Related Work

This paper studies designing a pose detector given the limited labeled data by leveraging multiview epipolar geometry and temporal consistency. These two supervisory signals are by large studied in isolation.

Temporal Supervision The tracking results such as optical flow [3], MOSSE [5] and discriminative correlation filters [12], provides an auxiliary information that can be used to enforce the temporal consistency across a continuous sequence [8, 31]. A challenge is that it suffers from tracking drift induced by object deformation, which substantially limits its validity. Such challenge has been addressed by learning the temporal evolution of tracking patches [18, 22] using recurrent neural networks. This generates a compromised network that minimizes the inconsistency in the learned trajectories, which suppresses the low-quality detection from the tracking drift. A pitfall of this approach is the requirement of per-frame annotation to supervise the recurrent network. This requirement can be relaxed by using supervision-by-registration approach [8] that achieves higher detection rate even with the limited labeled data. However, its application towards the pose detection for non-human species is still challenging because: (1) supervision from optical flow involves with the tracking drift caused by occlusion, and therefore, long-term tracking is infeasible; (2) the soft-argmax operation for computing

the track coordinate may lead to noisy supervision in the cases where the pose detection is erroneous (e.g., multiple peaks) as shown in the right inset figure. This multi-modality of pose recognition escalates when the keypoint is invisible. This strongly influences tracking accuracy, especially for a small-sized target; (3) the argmax operation takes into account only for the peak location where the non-maximum local peaks may play a role.



Multiview Supervision Multiview images possess highly redundant yet distinctive visual information that can be used to self-supervise the unlabeled data. Bootstrapping is a common practice: to use multiview images to robustly reconstruct the geometry using the correspondences and to project to the unlabeled images to provide a pseudo-label, which has been shown highly effective [6, 25, 29]. A pitfall of this approach is that it involves with an iterative process over learning and reconstruction. Another approach is to separately learn depth from a single view image in isolation that can be used for self-supervision [15, 27, 33]. This relies on the depth prediction where the accuracy of the trained model is bounded by the accuracy of reconstruction/prediction. Jafarian et al. [13] introduces a new framework that bypasses 3D reconstruction during the training process through the epipolar constraint, i.e., the epipolar constraint is transformed to the distribution matching. The problem of this approach is that its performance is highly dependent on the pre-trained model. It has no reasoning about outliers, i.e., the recognition network converges to a trivial solution if the outliers dominate the distribution of the multiview pose detection.

Our main hypothesis is that these two supervisions are complementary. We formulate the spatiotemporal supervision that can benefit from both and address each limitation. (1) We use dense optical flow tracking to address noisy supervision, i.e., it is unlikely that the noisy prediction is temporally correlated. (2) We leverage the end-to-end epipolar distribution matching to avoid the multimodality issue that arises using the soft-argmax operation. This is differentiable, and therefore, trainable. (3) The multiview image streams can alleviate the tracking drift [14, 32], i.e., it is unlikely that the tracking drift occurs in a geometrically consistent fashion. (4) Visibility map can assist to determine the validity of the tracking without explicit outlier rejection.

3. Multiview Supervision by Registration

Consider synchronized multiview image streams, $\mathcal{I} = \{\mathbf{I}_t^i\}$ where \mathbf{I}_t^i is the image of the i^{th} camera at t time instant. We denote the set of synchronized images at t time instant across all cameras with $\mathcal{I}_t = \{\mathbf{I}_t^1, \dots, \mathbf{I}_t^n\}$ where n is the number of cameras, and the set of images from the i^{th}

camera for all time instances with $\mathcal{I}^i = \{\mathbf{I}_1^i, \dots, \mathbf{I}_T^i\}$ where T is the total time instances. The images in \mathcal{I}_t satisfy epipolar geometry and the images in \mathcal{I}^i can be reliably tracked as the viewpoint does not change¹. Among these images, the annotations of body keypoints are available for a subset of images (2~3) at two end frames, i.e., $\mathcal{I}_L = \mathcal{J}_1 \cup \mathcal{J}_T$ where \mathcal{I}_L is the set of the labeled images, $\mathcal{J}_1 \subseteq \mathcal{I}_1$ and $\mathcal{J}_T \subseteq \mathcal{I}_T$ are the labeled subset of images at the first and end time instances. The set of the unlabeled images are denoted as $\mathcal{I}_U = \mathcal{I} \setminus \mathcal{I}_L$.

Given \mathcal{I}_L and \mathcal{I}_U , we formulate a flexible and differentiable semi-supervised learning framework that uses the complementary relationship between epipolar geometry (spatial constraint) and visual tracking (temporal coherence). We train a pose detector, $\phi(\mathbf{I}; \mathbf{w}) \in [0, 1]^{W \times H \times C}$ that produces a per-pixel probability² of being a keypoint where W , H , and C are the width, height, and the number of keypoints including the background. The pose detector is parametrized by the weight \mathbf{w} that is learned by minimizing the following loss:

$$L = \sum_{\mathbf{I} \in \mathcal{I}_L} L_L(\mathbf{I}) + \lambda_S \sum_{t=1}^T L_S(\mathcal{I}_t) + \lambda_T \sum_{i=1}^n L_T(\mathcal{I}^i), \quad (1)$$

where \mathcal{L}_L , \mathcal{L}_S , and \mathcal{L}_T are the losses for labeled supervision, multiview cross-supervision, and tracking supervision, and λ_S and λ_T are the weights that control their importance.

For the labeled data at the two end time instances, we use the Euclidean error to measure the loss for labeled supervision:

$$L_L(\mathbf{I}) = \|\mathbf{Y}_\mathbf{I} - \phi(\mathbf{I}; \mathbf{w})\|^2, \quad (2)$$

where $\mathbf{Y}_\mathbf{I} \in \{0, 1\}^{W \times H \times C}$ is the ground truth label of the labeled image \mathbf{I} .

3.1. Multiview Cross-supervision

Consider a 3D keypoint $\mathbf{X} \in \mathbb{R}^3$ at t time instant that is projected onto the i^{th} and j^{th} images (\mathbf{I}_t^i and \mathbf{I}_t^j) to form the 2D projections $\mathbf{x}_i, \mathbf{x}_j \in \mathbb{R}^2$. These projections to form keypoint on the images must satisfy the following:

$$\begin{aligned} \tilde{\mathbf{x}}_i &\cong \mathbf{P}_i \tilde{\mathbf{X}}, \quad \text{where } \mathbf{x}_i = \underset{\mathbf{x}}{\operatorname{argmax}} P^i(\mathbf{x}) \\ \tilde{\mathbf{x}}_j &\cong \mathbf{P}_j \tilde{\mathbf{X}}, \quad \text{where } \mathbf{x}_j = \underset{\mathbf{x}}{\operatorname{argmax}} P^j(\mathbf{x}) \end{aligned} \quad (3)$$

¹We consider a stationary multi-camera system [14, 32] while the spatiotemporal constraint of epipolar geometry and temporal coherence still applies for a moving synchronized multi-camera system, e.g., social cameras [2].

²Some pose detectors [26] directly regress the keypoint coordinates, which has been shown under-performance comparing to the probability output format [20, 30]. Nonetheless, the coordinate regressor can be also integrated in our semi-supervised framework with a trivial modification.

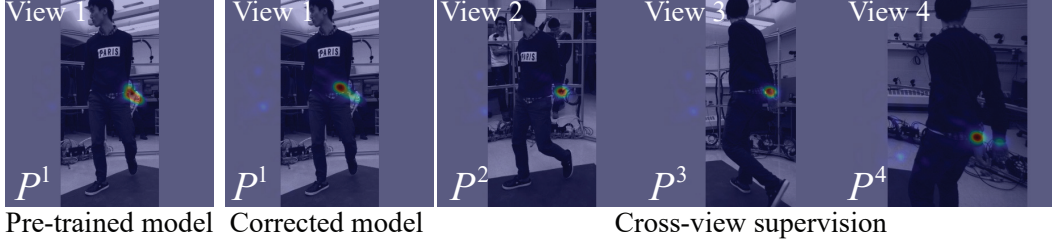


Figure 2: We leverage a multiview cross-supervisory signal to supervise each other’s view. With a pre-trained model, the hand location is erroneous because of occlusion. This occluded hand location can be corrected by reasoning about the visibility, i.e., the hand is fully visible from other views (view 2, 3, and 4), which produces geometrically consistent supervision to view 1.

where $\mathbf{P} \in \mathbb{R}^{3 \times 4}$ is the camera projection matrix, and $\tilde{\mathbf{x}}$ is the homogeneous representation of \mathbf{x} [11]. Note that the projection must agree with the keypoint detection where $P^i : \mathbb{R}^2 \rightarrow [0, 1]$ is the probability distribution given the i^{th} image computed by the keypoint detector, i.e., $P^i(\mathbf{x}) = \phi(\mathbf{I}^i; \mathbf{w})|_{\mathbf{x}}$. Equation (3) links multiple views through the 3D point where geometric consistency can be enforced in training the pose detector.

However, with Equation (3), the network cannot be trained due to the non-differential nature of the *argmax* operation³. This leads to alternating reconstruction [4, 6, 25, 29] or data driven depth prediction [15, 27, 33] that suffer from suboptimality.

Recently, Jafarian et al. [13] have shown that it is possible to transform the probability map to produce the distribution of epipolar lines in the other view:

$$P^{j \rightarrow i}(\mathbf{x}_i) = \sup_{\tilde{\mathbf{x}}^T \mathbf{F} \tilde{\mathbf{x}}_i = 0} P^j(\mathbf{x}) \quad (4)$$

where $P^{j \rightarrow i} : \mathbb{R}^2 \rightarrow [0, 1]$ is the probability distribution of the epipolar lines in the i^{th} image transferred from the j^{th} image, and \mathbf{F} is the fundamental matrix between the j^{th} and i^{th} images. See [13] for more details.

The key finding is that there exists 1D distribution that forms the equivalent epipolar constraint, i.e.,

$$\tilde{\mathbf{x}}_j^T \mathbf{F} \tilde{\mathbf{x}}_i = 0 \iff D_{\text{KL}}(Q_i || Q_{j \rightarrow i}) = 0 \quad (5)$$

where Q_i is the warped 1D probability of P^i and $Q_{j \rightarrow i}$ is the 1D probability of epipolar line transferred from P^j , and D_{KL} is KL divergence [16].

From Equation (5), we can derive the loss for multiview cross-supervision:

$$L_S(\mathcal{I}_t) = \sum_{i,j \in \mathcal{S}} D_{\text{KL}}(Q_i || Q_{j \rightarrow i}), \quad (6)$$

where \mathcal{S} is the camera index set of \mathcal{I}_t .

³As noted in Section 2, a soft-argmax operation for computing the coordinate often produces a multi-modal probability map, resulting in erroneous and noisy supervision.

3.2. Temporal Supervision

Within the i^{th} camera, the dense per-pixel trajectory provides a temporal supervisory signal, i.e., the keypoint detection \mathbf{x}_t at t time instant can supervise that of $t + 1$ time instant $\mathbf{x}_{t+1} = \mathbf{x}_t + \Delta \mathbf{x}$ where $\Delta \mathbf{x}$ is the optical flow between two frames. Given dense tracking, the image at t time instant can be approximated by $t + 1$, i.e., $\mathbf{I}_{t+1}^i(\mathbf{x}) \approx \mathbf{I}_t^i(W_{t+1 \rightarrow t}(\mathbf{x}))$ where $W_{t+1 \rightarrow t} : \mathbb{R}^2 \rightarrow \mathbb{R}^2$ is a warping field, or inverse compositional mapping (ICM). We use this dense warping to predict the keypoint probability:

$$P_{t+1}^i(\mathbf{x}) \approx P_t^i(W_{t+1 \rightarrow t}(\mathbf{x})), \quad (7)$$

where P_t^i and P_{t+1}^i are the keypoint probability maps of the i^{th} camera at t and $t + 1$ time instances.

Based on Equation (7), we design a loss for a temporal supervision:

$$L_T(\mathcal{I}^i) = \sum_{t_1, t_2 \in [0, T]} \sum_{\mathbf{x} \in \mathcal{X}} \|P_{t_1}^i(\mathbf{x}) - P_{t_2}^i(W_{t_1 \rightarrow t_2}(\mathbf{x}))\|^2$$

where \mathcal{X} is the domain of the i^{th} image.

3.3. Visibility Supervision

Self-occlusion frequently occurs in dynamic human body motion, which requires precise visibility reasoning for long term 3D body tracking [14]. RANSAC [9] has been used to filter out outliers and invisible keypoints from multiview image streams, which is not differentiable, and therefore, an end-to-end training is not feasible [25]. For our case, the visibility plays a pivotal role as the error induced by occlusion can propagate through cross-view and temporal supervisions. We integrate the visibility inference as a part of the training process. Consider a visibility map $V_t^i : \mathbb{R}^2 \rightarrow [0, 1]$. Using this visibility map, we condition on the probability of each keypoint:

$$P_t^i(\mathbf{x}) \leftarrow V_t^i(\mathbf{x}) P_t^i(\mathbf{x}), \quad (8)$$

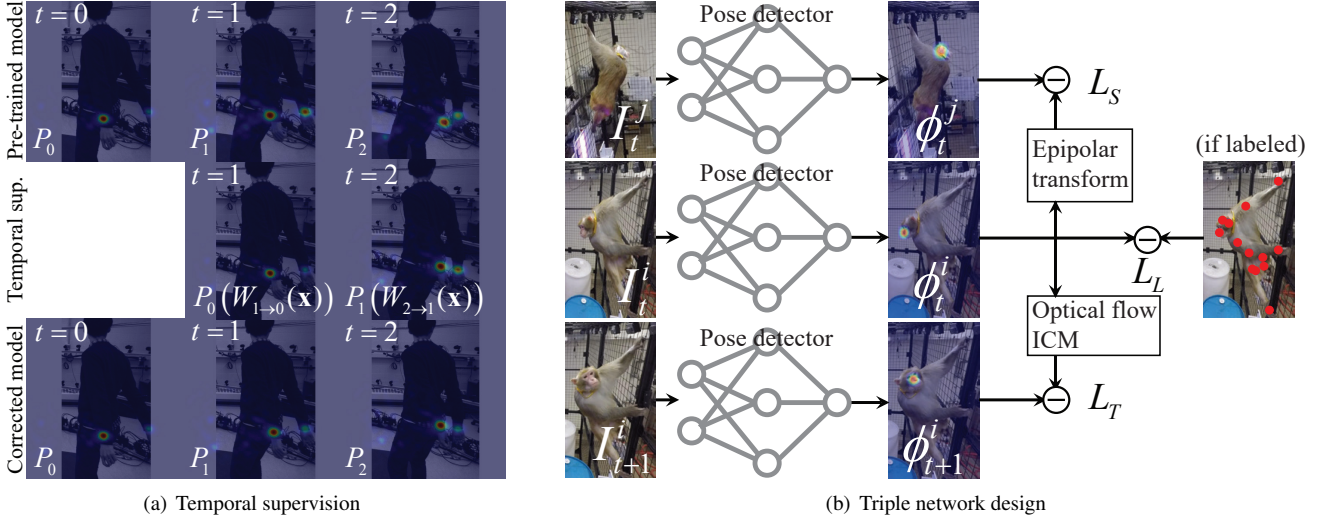


Figure 3: (a) We leverage a temporal supervisory signal using visual dense tracking to supervise between frames. (b) We design a triple network that learns a geometrically consistent and temporally coherent pose detector given a limited number of the labeled data. It minimizes the losses for label supervision (L_L), multiview cross-supervision (L_S), and temporal supervision via tracking (L_T). We use an abuse of notation: $\phi(\mathbf{I}_t^i) = \phi_t^i$.



Figure 4: We integrate a visibility inference to validate the multiview supervisory signals. The left hand is occluded by torso (left), which is conditioned by the visibility map (middle), resulting in the reduction of the keypoint probability. This prevents from influencing the occluded keypoint detection across views.

where the new probability is re-scaled according to the likelihood of visibility, i.e., if the keypoint is invisible at \mathbf{x} , $V(\mathbf{x}) = 0$, the probability is set to $P(\mathbf{x}) = 0$.

To compute the visibility map, we train another network $V_t^i(\mathbf{x}) = \psi(\mathbf{I}_t^i; \mathbf{w}_v)$ parametrized by \mathbf{w}_v using the labeled data. We augment Equation (2) to jointly train the keypoint detector and visibility:

$$L_L(\mathbf{I}) = \|\mathbf{Y}_I - \phi(\mathbf{I}; \mathbf{w})\|^2 + \|\mathbf{Z}_I - \psi(\mathbf{I}; \mathbf{w}_v)\|^2, \quad (9)$$

where $Z_I \in \{0, 1\}^{W \times H \times C}$ is the ground truth visibility of the labeled image \mathbf{I} obtained by ray-casting. Figure 4 illustrates the effect of the visibility map where the keypoint probability of left hand (left) is conditioned by the visibility map (middle), resulting in the reduction of the keypoint

probability. This prevents from influencing the occluded keypoint detection across views.

In addition, we apply a spatial prior on the visibility map. The key idea is that a keypoint is likely to be visible if it is visible from the nearby cameras. This provides a spatial prior similar to the multiview cross-supervision. We augment Equation (6) to reason about the visibility during the process of training:

$$L_S(\mathcal{I}_t) = \sum_{i,j \in \mathcal{S}} D_{\text{KL}}(Q_i \| Q_{j \rightarrow i}) + D_V(V_t^i, V_t^j), \quad (10)$$

where \mathcal{S} is the camera index set of \mathcal{I}_t .

$$D_V(V_t^i, V_t^j) = \delta_{i,j} \|\max V_t^i - \max V_t^j\|^2 \quad (11)$$

where $\delta_{i,j}$ is Kronecker delta that is one if the distance between the optical centers of the i^{th} and j^{th} cameras is smaller than ϵ_C , i.e., $\|\mathbf{C}_i - \mathbf{C}_j\| < \epsilon_C$, and zero otherwise.

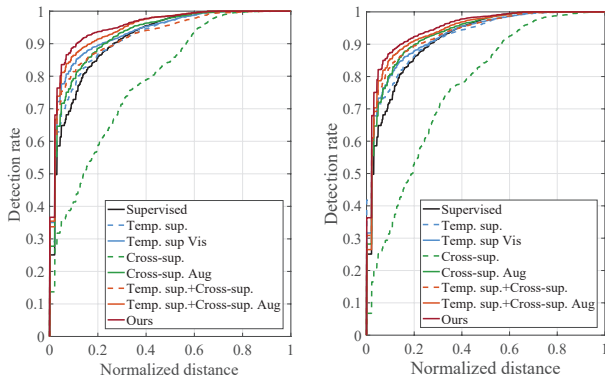
4. Implementation

We design a triple network based on a state-of-the-art pose detector [7] that leverages the multiview cross-supervision and temporal supervision as shown in Figure 3(b). The weights of pose detector (\mathbf{w}) and visibility map (\mathbf{w}_v) are learned. Each pose detector takes a single image with the size of $368 \times 368 \times 3$ and outputs the C probability map with $46 \times 46 \times 21$.

Network Initialization by Bootstrapping Given multiview image streams, we label a subset of images at the

Method	multiview Human Image Stream Dataset								multiview Dog dataset							
	Nec	Sho	Elb	Wri	Hip	Kne	Ank	AUC	Nose	Hea	Nec	F.Leg	Paw	Hip	H. Leg	AUC
Supervised	97.9	81.7	37.9	33.6	99.2	86.1	95.3	91.6	96.1	97.6	96.1	80.3	34.8	97.2	82.1	91.3
Temp. Sup. [8]	97.8	86.4	44.6	32.5	97.0	93.4	97.5	91.7	92.0	93.3	94.2	83.2	31.6	95.0	83.3	92.0
Temp. Sup vis.	97.9	92.7	48.4	41.1	97.6	97.8	98.6	93.3	98.7	97.2	96.9	91.5	38.1	96.3	88.9	92.5
Cross-sup. [13]	98.9	62.4	31.7	19.8	21.8	44.7	77.9	78.7	82.3	83.1	85.3	68.7	23.6	42.4	61.4	76.3
Cross-sup. aug.	99.4	85.0	41.5	38.6	98.0	97.6	86.1	92.6	98.5	95.3	96.6	88.2	35.3	97.1	91.2	92.9
Temp. sup.+Cross-sup.	99.7	88.8	70.6	40.2	99.8	97.5	97.8	92.2	99.2	98.2	96.1	89.1	37.2	98.5	92.3	92.9
Temp. sup.+Cross-sup. aug	94.3	89.4	77.1	57.5	98.9	98.6	99.8	92.2	97.1	97.3	98.9	92.5	52.8	96.9	95.8	93.8
Ours	97.2	92.9	77.2	65.4	98.9	98.9	99.8	95.1	96.2	99.1	98.9	94.2	53.2	96.9	95.8	94.8

Table 1: Quantitative results of human activity: Keypoint detection performance of different methods measured on each joint by the metric PCKh. PCK with full-ranged threshold is used to measure AUC.



(a) PCK of human subject.

(b) PCK of dog subject.

Figure 5: The PCK evaluates 8 methods for two subjects: human and dog. Our approach outperforms the supervised method, 2 unsupervised baselines and 4 of their variant.

first and end time instances. The fundamental matrices between cameras and the dense trajectories between frames are precomputed. To alleviate the noisy initialization of the detector, which occurs frequently when the unlabeled data dominate, we take a few practical steps. (1) With a subset of labeled data in the same time instant, we triangulate the keypoint in 3D with RANSAC. This 3D keypoint is projected onto all multiview images, which can greatly augment the labeled data reliably. (2) Based on the 3D pose with volume estimation, we compute the visibility using ray-casting, which provides the visibility map label for all views. (3) With the augmented labeled data with their visibility, we train a pose detector in a fully supervised manner. (4) Using the pre-trained model, we detect the keypoints on the unlabeled data, and then, triangulate in 3D and project back onto the multiview unlabeled data to get their pseudo-labels. (5) We re-train the pre-trained network with the unlabeled data with their pseudo-labels. (6) This process is called bootstrapping [25], which provides a good initialization to train our triple network.

Data and Network Setting The choice of the multiview pairs play a major role because there exists a degenerate case if the all cameras lie in a co-planar surface [13]. To

avoid this, we select the pairs that have different height of cameras. The temporal pairs include all pairs of consecutive frames and pair between the labeled data and unlabeled data to minimize the effect of tracking drift. We implement this neural network with Tensorflow on nVidia GTX 1080. Adam optimizer with $\alpha = 10^{-4}$, 0.95 decay rate, and 5000 decay steps is used.

5. Experiments and Results

We evaluate our approach using realworld multiview image streams without a pre-trained model captured by two different multi-camera systems. (1) A multiview behavioral imaging system composed of 69 synchronized HD cameras capture human activities at 30 fps with 1024×1280 resolution. We select 51 consecutive synchronized frames from 10 camera as training streams. Two end frames are used for the labeled data (20 images) and the rest images are used for the unlabeled data (490). The human pose detectors are used to triangulate the 3D pose to provide the ground truth. (2) Another multi-camera system composed of 69 synchronized HD cameras are used to capture dog behaviors. The scenes are recorded at 15 fps with 1024×1280 resolution. The ground truth labels are manually annotated across time. (3) A monkey behavioral imaging system composed of 35 cameras running at 60 fps are used to measure monkey activities. The camera produces 1280×960 resolution images. The ground truth is manually labeled.

5.1. Evaluation

We compare our method with three major approaches: (1) fully supervised learning with the labeled data; (2) semi-supervised learning with temporal supervision [8]; (3) semi-supervised learning with multiview cross-supervision [13]. We use the probability of correct keypoint (PCK) for the evaluation metric. Figure 8 illustrates keypoint detection results produced by our trained detector to the other methods. We also compare with four variant of our approaches: (a) semi-supervised learning with multiview cross-supervision where cross-supervision is boosted by data augmentation (b) semi-supervised learning with temporal supervision where temporal supervision is boosted by visibility of key-

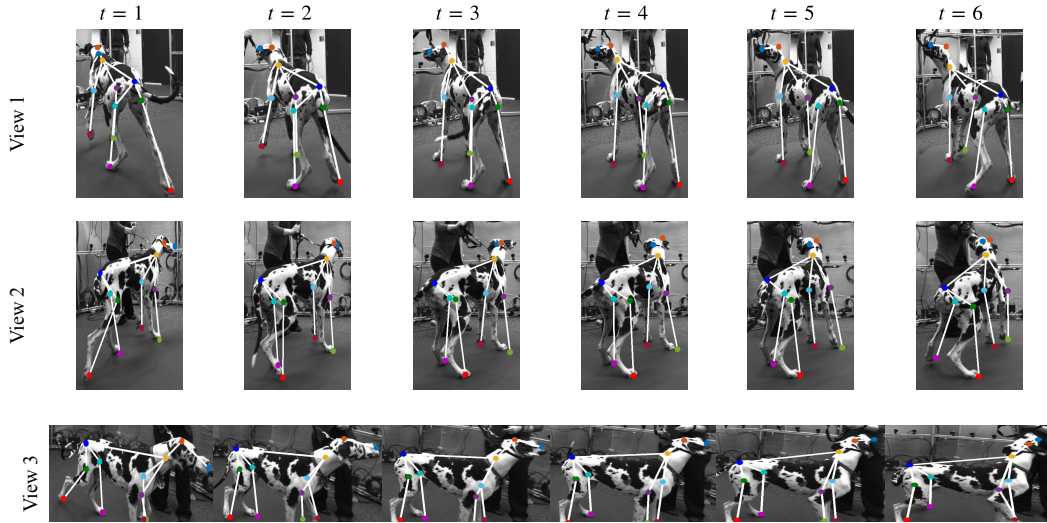


Figure 6: Qualitative results of dog activity

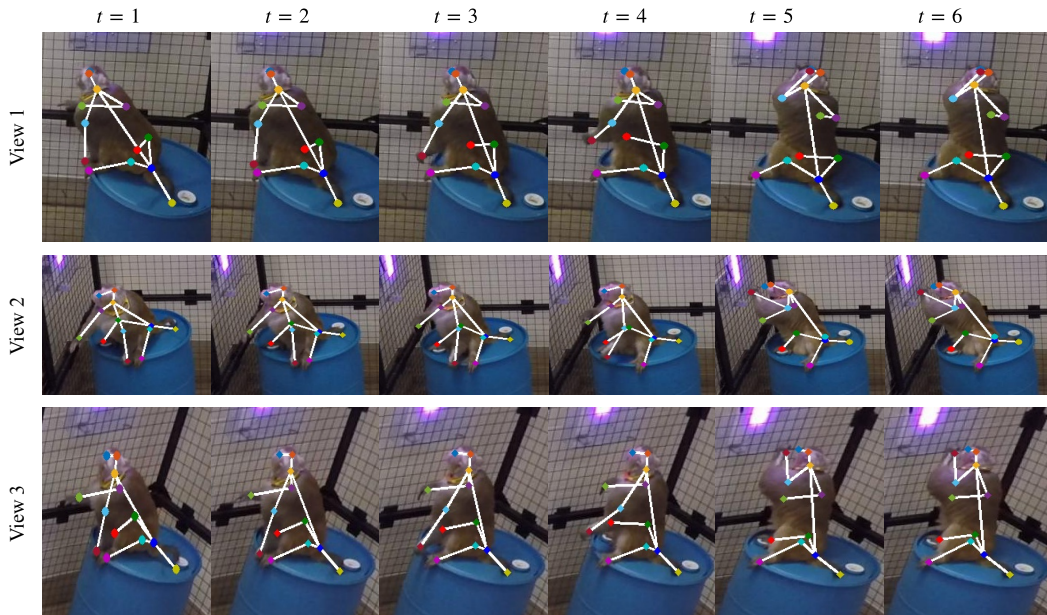


Figure 7: Qualitative results of monkey activity

point (c) semi-supervised learning with temporal supervision [8] and multiview cross-supervision [13] (d) semi-supervised learning with temporal supervision [8] and data augmentation-assisted multiview cross-supervision [13]

Figure 6, 7 and 8 show qualitative comparison among the supervised method, two unsupervised baselines, three main variant of the unsupervised methods and out method. Ours outperforms others in full-ranged PCK metric. Specifically, multiview cross-supervision achieve worse performance than all others, while data augmentation boosts it; temporal supervision, applied to supervised method, only achieves minor improvement in short distance, and even

worsen detection in large distance, while visibility probability improves temporal supervision by enhancing detection rate in larger distance.

Table 1 quantitatively compares our keypoint detection results against the supervised method and other unsupervised methods. The table reports PCKh [1] of each joint and Area under Curve (AUC) computed for the entire range of PCK thresholds. Our approach achieves 95.1% on the Human dataset and 94.8% AUC on the Dog dataset, which outperforms the other 2 unsupervised baselines, temporal supervision [8] and multiview cross-supervision [13], by 3.4% and 16.4% AUC respectively on the Human dataset,



Figure 8: Qualitative results of human activity

and by 2.8% and 18.8% AUC on the Dog dataset. In addition, visibility probability improves temporal supervision by 1.8% AUC on the Human dataset and 2.65% AUC on the Dog dataset, and it also wins over PCKh evaluation on the occluded-prone keypoints. Similarly, data augmentation improves cross-supervision by 16.6% AUC on the Human dataset and 13.9% AUC on the Dog dataset.

6. Summary

We proposed a novel unsupervised framework to improve keypoint detection in videos from multiview system.

Our main contribution is to (1) encode both temporal constraint and spatial constraint into multiview keypoint detector, where both constraints can be extracted in an unsupervised fashion, (2) correct the inaccurate extracted representation of temporal supervision and multiview cross-supervision by supervising each other, and (3) learn visibility of keypoint based on the labeled data and incorporate the visibility into temporal supervision. The proposed method is proved providing the detector with large improvement even with extremely low proportion of the labeled data.

References

- [1] M. Andriluka, L. Pishchulin, P. Gehler, and B. Schiele. 2d human pose estimation: New benchmark and state of the art analysis. In *CVPR*, 2014.
- [2] I. Arev, H. S. Park, Y. Sheikh, J. K. Hodgins, and A. Shamir. Automatic editing of footage from multiple social cameras. *SIGGRAPH*, 2014.
- [3] S. Baker and I. Matthews. Lucas-kanade 20 years on: A unifying framework. *IJCV*, 2004.
- [4] G. Bertasius, S. X. Yu, H. S. Park, and J. Shi. Exploiting visual-spatial first-person co-occurrence for action-object detection without labels. In *ICCV*, 2017.
- [5] D. S. Bolme, J. R. Beveridge, B. A. Draper, and Y. M. Lui. Visual object tracking using adaptive correlation filters. In *CVPR*, 2010.
- [6] A. Byravan and D. Fox. SE3-nets: Learning rigid body motion using deep neural networks. In *ICRA*, 2016.
- [7] Z. Cao, T. Simon, S.-E. Wei, and Y. Sheikh. Realtime multi-person 2d pose estimation using part affinity fields. *CVPR*, 2016.
- [8] X. Dong, S.-I. Yu, X. Weng, S.-E. Wei, Y. Yang, and Y. Sheikh. Supervision-by-registration: An unsupervised approach to improve the precision of facial landmark detectors. In *CVPR*, 2018.
- [9] M. A. Fischler and R. C. Bolles. Random sample consensus: A paradigm for model fitting with applications to image analysis and automated cartography. *ACM Comm.*, 1981.
- [10] Y. Furukawa and J. Ponce. Dense 3d motion capture from synchronized video streams. In *CVPR*, 2008.
- [11] R. Hartley and A. Zisserman. *Multiple View Geometry in Computer Vision*. Cambridge University Press, second edition, 2004.
- [12] J. F. Henriques, R. Caseiro, P. Martins, and J. Batista. High-speed tracking with kernelized correlation filters. *TPAMI*, 2015.
- [13] Y. Jafarian, Y. Yao, and H. S. Park. Monet: Multiview semi-supervised keypoint via epipolar divergence. *arXiv*, 2018.
- [14] H. Joo, H. S. Park, and Y. Sheikh. Map visibility estimation for large-scale dynamic 3d reconstruction. In *CVPR*, 2014.
- [15] A. Kanazawa, M. J. Black, D. W. Jacobs, and J. Malik. End-to-end recovery of human shape and pose. In *CVPR*, 2018.
- [16] S. Kullback and R. A. Leibler. On information and sufficiency. *Annals of Mathematical Statistics*, 1951.
- [17] T.-Y. Lin, M. Maire, S. Belongie, J. Hays, P. Perona, D. Ramanan, P. Dollár, and C. L. Zitnick. Microsoft coco: Common objects in context. In *ECCV*, 2014.
- [18] H. Liu, J. Lu, J. Feng, and J. Zhou. Two-stream transformer networks for video-based face alignment. *TPAMI*, 2018.
- [19] A. Mathis, P. Mamidanna, K. M. Cury, T. Abe, V. N. Murthy, M. W. Mathis, and M. Bethge. Deeplabcut: markerless pose estimation of user-defined body parts with deep learning. *Nature Neuroscience*, 2018.
- [20] A. Newell, K. Yang, and J. Deng. Stacked hourglass networks for human pose estimation. In *ECCV*, 2016.
- [21] D. Paschalidou, A. O. Ulusoy, C. Schmitt, L. van Gool, and A. Geiger. Raynet: Learning volumetric 3d reconstruction with ray potentials. In *CVPR*, 2018.
- [22] X. Peng, R. S. Feris, X. Wang, and D. N. Metaxas. A recurrent encoder-decoder network for sequential face alignment. In *ECCV*, 2016.
- [23] A. Poms, C. Wu, S.-I. Yu, and Y. Sheikh. Learning patch reconstructability for accelerating multi-view stereo. In *CVPR*, 2018.
- [24] C. Shin, H.-G. Jeon, Y. Yoon, I. S. Kweon, and S. J. Kim. Epinet: A fully-convolutional neural network using epipolar geometry for depth from light field images. In *CVPR*, 2018.
- [25] T. Simon, H. Joo, I. Matthews, and Y. Sheikh. Hand keypoint detection in single images using multiview bootstrapping. In *CVPR*, 2017.
- [26] A. Toshev and C. Szegedy. Deeppose: Human pose estimation via deep neural networks. In *CVPR*, 2014.
- [27] S. Tulsiani, T. Zhou, A. A. Efros, and J. Malik. Multi-view supervision for single-view reconstruction via differentiable ray consistency. In *CVPR*, 2017.
- [28] M. Velliste, S. Perel, M. C. Spalding, A. S. Whitford, and A. B. Schwartz. Cortical control of a prosthetic arm for self-feeding. *Nature*, 2008.
- [29] S. Vijayanarasimhan, S. Ricco, C. Schmid, R. Sukthankar, and K. Fragkiadaki. Sfm-net: Learning of structure and motion from video. In *arXiv*, 2017.
- [30] S.-E. Wei, V. Ramakrishna, T. Kanade, and Y. Sheikh. Convolutional pose machines. In *CVPR*, 2016.
- [31] A. G. Xiaolong Wang. Unsupervised learning of visual representations using videos. In *ICCV*, 2015.
- [32] J. S. Yoon, Z. Li, and H. S. Park. 3d semantic trajectory reconstruction from 3d pixel continuum. In *CVPR*, 2017.
- [33] T. Zhou, M. Brown, N. Snavely, and D. G. Lowe. Unsupervised learning of depth and ego-motion from video. In *CVPR*, 2017.
- [34] X. Zhu, C. Vondrick, C. C. Fowlkes, and D. Ramanan. Do we need more training data? *IJCV*, 2015.